Thus the major differences in glass temperature are attributed to differences in conformational entropies due to differences in conformational energies and configurational entropies associated with the packing of chains in the liquid.

Acknowledgment. We are grateful to A. E. Tonelli for making the entropy calculations based on the RIS model and discussing those results with us.

References and Notes

(1) Gibbs, J. H.; DiMarzio, E. A. *J. Chem. Phys.* **1958**, *28*, 373.
(2) Passaglia, E.; Kevorkian, H. *J. Appl. Phys.* **1965**, *34*, 90.
(3) Karasz, F. E.; Bair, H. E.; O'Reilly, J. M. *J. Phys. Chem* **1965**, *69*, 2657.
(4) Fox, T. G.; Garret, B. S.; Goode, W. E.; Gratch, S.; Kincaid, J. F.; Spell, A.; Stroupe, J. D. *J. Am. Chem. Soc.* **1958**, *80*, 1768.
(5) Karasz, F. E.; O'Reilly, J. M. *Rev. Sci. Instrum.* **1966**, *37*, 255.
(6) Sochava, I. V.; Trapeznikova, O. N. *Vestn. Leningr. Univ. Ser. Fiz. Khim.* **1958**, *13*, 65.
(7) McCrum, G.; Read, B. E.; Williams, G. "Anelastic Processes in Polymers"; Wiley: New York, 1967.
(8) Slichter, W. P. *NMR Basic Princ. Prog.* **1971**, *4*, 209–231.
(9) O'Reilly, J. M.; Karasz, F. E. *J. Polym. Sci., Part C* **1966**, *14*, 49.
(10) Wittman, J.; Kovacs, A. J. *J. Polym. Sci., Part C* **1975**, *16*, 4443.
(11) Roe, J. M.; Simha, Robert. *Int. J. Polym. Mater.* **1975**, *3*, 193.
(12) Sharanov, Y. A.; Volkenstein, M. V. *Solid State Phys.* **1963**, *5*, 590.
(13) Petrie, S. E. B.; Marshall, A. K. *J. Appl. Phys.* **1975**, *46*, 4223.
(14) O'Reilly, J. M.; Karasz, F. E. *Polym. Prepr., Am. Chem. Soc., Div. Polym. Sci.* **1964**, *5* (2), 351.
(15) Beatty, C. L.; Karasz, F. E. *Org. Coat. Plast.* **1975**, *35*, 370.
(16) Beck, D. L.; Hiltz, A. A.; Knox, J. R. *SPE Trans.* **1963**, *3*, 1.
(17) Hellwege, K. H.; Hennig, J.; Knappe, W. *Kolloid Z. Z. Polym.* **1962**, *186*, 29.
(18) Kusy, R. P. *J. Polym. Sci., Polym. Chem. Ed.* **1976**, *14*, 1527.
(19) Sundararajan, P. R.; Flory, P. J. *J. Am. Chem. Soc.* **1974**, *96*, 5025.
(20) Tonelli, A. E., private communication.
(21) O'Reilly, J. M.; Mosher, R. A. *Macromolecules* **1981**, *14*, 602.
(22) Goldstein, M. *J. Chem. Phys.* **1976**, *64*, 4767.
(23) Chang, S. S.; Bestul, P. B. *J. Chem. Phys.* **1972**, *56*, 503.

Stability of the Cross-Linked Tropomyosin Dimer: Cross-Link Effect on the Cooperativity of the Ordering Process and on the Maximum in the Helix Probability Profile

Wayne L. Mattice* and Jeffrey Skolnick†

Department of Chemistry, Louisiana State University, Baton Rouge, Louisiana 70803.
Received December 11, 1981

ABSTRACT: A configuration partition function has been formulated for a partially helical, cross-linked, in-register dimer composed of polypeptide chains of identical degree of polymerization. The three important features incorporated in this formulation are as follows: (1) Conformational flexibility is allowed in the cross-linking unit, with certain of the cross-link configurations giving rise to nonalignment of helices propagating away from the cross-link site. (2) Cross-linking of the helices may be accompanied by deformation of the helices near the cross-link site (or may induce stress in the cross-linking unit). (3) There is assumed to be a vanishingly small probability that a sequence of random coil residues connecting two helical segments will adopt a configuration that causes the helical segments to be collinear. Application is made to the case of cross-linked α-tropomyosin. Features 1 and 2, which are indistinguishable in this formulation of the configuration partition function, are found to have a profound impact on the high-temperature portion of the thermal denaturation of the cross-linked dimer. Feature 3 has two important consequences for the helix probability profile in the middle of the thermal denaturation: local detail, seen at low helicity, is obscured, and the maximum in the helix probability profile is shifted to the residue at the cross-link site. Thus conclusions as to the most stable helical region in the cross-linked dimer will be affected by the incorporation of feature 3 into the configuration partition function.

Dimeric tropomysin has a helical content greater than 90% in physiological media at low temperatures.[1-7] Helix–coil transition theory indicates that monomeric tropomyosin at low temperature should have a helical content in the vicinity of 17%.[8] A logical inference is that helix–helix interaction constitutes the major factor responsible for the high helicity of the dimeric form.[9-12] This extra stabilization can be overcome by an appropriate increase in temperature, as is shown by the observation of thermal denaturation for the cross-linked dimer of tropomyosin.[4,5] These features of the behavior of tropomyosin have been rationalized by a theoretical treatment of the helix–coil transition in in-register, two-chain, coiled-coil polypeptides that may or may not be cross-linked.[13] The objective here is to explore consequences of several refinements in the theoretical treatment, with special emphasis on their implications for the thermal denaturation of cross-linked tropomyosin.

Pertinent aspects of the original treatment are conveniently presented with the aid of schematics A and B of Figure 1. Figure 1A schematically depicts two identical helical chains cross-linked via a disulfide bond. Helices, which are depicted as thin rods, are parallel and in register. Separation of the two helices is assumed to be so small that residue i in one chain interacts with residue i on the other chain. This interaction is represented by the dashed line drawn for the residue denoted by the arrow to its partner on the other chain. Figure 1B depicts a configuration in which the tail of one chain is in the random coil state. It is assumed that the disordered segment does not interact with the other polypeptide chain. We now focus on contributions made to the statistical weight of each configu-

† Present address: Department of Chemistry, Washington University, St. Louis, MO 63130.

0024-9297/82/2215-1088$01.25/0

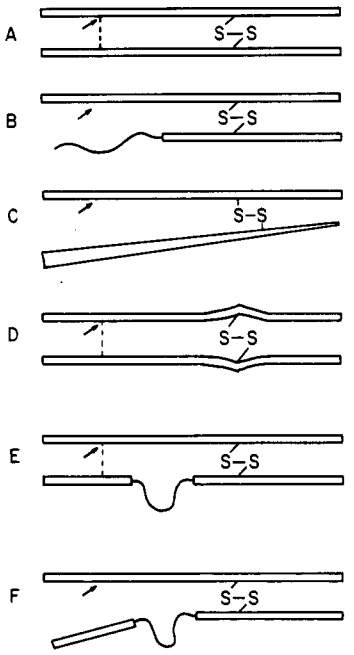

Figure 1. Six schematic configurations of a cross-linked dimer.

ration by the amino acid residue at the position denoted by the arrow, as well as its partner on the other chain. Statistical weights potentially accessible to each amino acid residue are assumed to include those described by Zimm and Bragg.[14] In Figure 1B, the indicated residue in the top chain is in the interior of a helical segment, and its statistical weight is therefore s_i. The corresponding residue in the other chain is in a random coil segment. It therefore has statistical weight of unity. Since the residues do not interact, their combined contribution to the statistical weight of the configuration in Figure 1B is simply the factor s_i. Both residues are in the interior of a helical segment in the configuration depicted in Figure 1A. If the helices did not interact, these two residues would contribute a factor s_i^2 to the statistical weight of this configuration. When the two residues interact, their contribution becomes $s_i^2 w_i$, where w_i is the factor that arises from that interaction. Values of w_i only slightly greater than unity will suffice to produce an almost completely helical dimer under conditions where the helicity of monomers is small.

The situation depicted in Figure 1A is an oversimplification; not every residue in the real tropomyosin dimer is in contact with its counterpart on the adjacent chain. In order to effect the stabilization represented by w, residues a and d, or e and g, of the quasi-repeating abcdefg heptet must be in contact with d′ and a′, or g′ and e′, on the neighboring chain. These contacts are present only if all residues a–d (or e–g) are in the helical conformation. Our original treatment[13] accounted for this requirement by the introduction of the coarse-graining approximation in which tropomyosin was divided into alternating four- and three-member blocks, i.e., the 4,3 approximation. However, for the values of σ and s appropriate to the primary structure of tropomyosin, even for noninteracting chains the average length of a helical sequence is 16 residues. If the helix–helix interaction parameter per block is assumed to be site independent, then the stabilization per block is found to be equal to $w_i^{3.5}$, with w_i the stabilization per residue calculated in the single-interacting residue pair approximation. Thus for convenience we shall employ the single-interacting residue pair approximation, although coarse graining permits a more detailed treatment of the actual interchain interactions present in this protein.

The refinements to be discussed here are easily described with the aid of Figure 1C–F. Figure 1C shares with Figure 1A the feature that cross-linked chains are completely helical. However, the conformation of the cross-link is assumed to be different in these two configurations. As a consequence, helices in Figure 1C are not aligned, and the residue denoted by the arrow cannot participate in an interaction with its partner on the other chain. The statistical weight contributed by this pair of residues is $s_i^2 w_i$ for the configuration in Figure 1A, but it is just s_i^2 for the configuration depicted in Figure 1C. One objective here is to explore the consequences of distinguishing between configurations depicted in schematics A and C of Figure 1.

In Figure 1D both cross-linked chains are completely helical, and the helices are aligned so that an interaction takes place between the residue denoted by the arrow and its partner on the other chain. These two residues therefore contribute a factor $s_i^2 w_i$ to the statistical weight of this configuration. However, alignment of the helices is assumed to have required the imposition of a stress at the cross-link site. In addition, the configurational entropy of the cross-linked molecules is reduced. Another objective is to inquire how this stress might modify the helicity of the cross-linked dimer.

Schematics 1E and 1F depict configurations of cross-linked dimers in which a random coil segment occurs within one of the chains. In Figure 1E, both helical segments are assumed to have maintained alignment with their partners on the completely helical chain. This alignment could occur only at the expense of the configurational entropy of the random coil segment, i.e., the loop entropy. These configurations are a priori excluded in the formulation presented below. Evaluation of the full model that includes loop entropy indicates neglect of these configurations has no important consequences in the present case.[15] We retain configurations such as that depicted in Figure 1F, where the random coil segment is unconstrained. Now the helical segment at the tail of the bottom chain is not in a position to interact with the other chain. The residue denoted by the arrow and its partner on the other chain contribute a statistical weight of $s_i^2 w_i$ to the configuration depicted in Figure 1E, but their contribution is only s_i^2 for the configuration depicted in Figure 1F. A final objective is to ascertain the impact of configurations such as that depicted in Figure 1F upon the properties of the cross-linked dimer.

Configuration Partition Function

We assume two polypeptide chains with amino acid residues indexed 1 through n. While the present application assumes the chains have identical amino acid sequences, extension to the case where the amino acid sequences differ is straightforward. In order to differentiate the chains from one another, we label them A and B. A cross-link is present between residues A_x and B_x.

The states potentially available to each residue are denoted c, h, and h*. The configuration of a residue must be that found in the helix if its state is to be h or h*; any other configuration is denoted by c. States denoted by h* differ from those denoted by h in that they merit an additional weighting factor that arises from helix–helix interaction in the cross-linked dimer.

All residues can occupy a c state by simply adopting the appropriate internal conformation. Whether the h or h* state is also accessible depends on events elsewhere in the cross-linked dimer. Residue A_i can occupy the h* state only if residues A_i through A_x are helical, the cross-link has a configuration that aligns the helices, *and* residues B_i

through B_x are helical. If these conditions are all met simultaneously, residue A_i can occupy the h* state but cannot be in the h state. If any of these conditions is not fulfilled, the h state is accessible but the h* state is not. If $x < i$, we must look backward along the chain from residue i in order to ascertain whether the h* state is accessible. However, if $i < x$, we must then look forward along the chain in order to make this determination. The requirement that we be able to look forward means that our formulation cannot be based on the 2×2 version of the Zimm–Bragg statistical weight matrix. In that matrix, rows index the state of residue $i - 1$ and columns index the state of residue i. There is no information about the state occupied by residue $i + 1$. We will instead have to build upon a 3×3 version of that matrix in which rows index the states of residue $i - 1$ and i, while columns index the states of residues i and $i + 1$.[13]

$$\mathbf{U}_i^{3\times 3} = \begin{bmatrix} 1 & 0 & \sigma^{1/2}s \\ 1 & 0 & 0 \\ 0 & \sigma^{1/2}s & s \end{bmatrix}_i \tag{1}$$

The order of indexing is c(c or h), hc, hh. A residue at either end of a helical segment merits a statistical weight of $\sigma_i^{1/2}s_i$, and the use of zero for the 1, 2 element prohibits the occurrence of helical segments containing only one residue.

The required statistical weight matrices for the A_iB_i pair are of dimensions 10×10 and are of different formulation depending upon whether $i < x$, $i = x$, or $i > x$. The strategy involved in their formulation is perhaps more easily described if the initial dimensions are 20×20. Condensation of the larger matrix gives rise to the matrices actually used in the computations. Rows are indexed by states for residues $i - 1$ and i in chains A and B, while columns are indexed by states of residues i and $i + 1$. If each residue could be c or h and if condensation is not effected, the dimensions are $2^4 \times 2^4$ (16×16). Dimensions increase to 20×20 when h* states are included. When $i < x$, indexing must include the four following possibilities: $(ch^*)_A(ch^*)_B$, $(hh^*)_A(ch^*)_B$, $(ch^*)_A(hh^*)_B$, and $(h^*h^*)_A(h^*h^*)_B$. The four added possibilities are $(h^*c)_A(h^*c)_B$, $(h^*h)_A(h^*c)_B$, $(h^*c)_A(h^*h)_B$, and $(h^*h^*)_A(h^*h^*)_B$ when $i > x$. Finally, when $i = x$, the four added rows are indexed $(ch^*)_A(ch^*)_B$, $(hh^*)_A(ch^*)_B$, $(ch^*)_A(hh^*)_B$, and $(h^*h^*)_A(h^*h^*)_B$, but the four additional columns are indexed $(h^*c)_A(h^*c)_B$, $(h^*h)_A(h^*c)_B$, $(h^*c)_A(h^*h)_B$, and $(h^*h)_A(h^*h)_B$. In all cases the resulting matrix is 20×20. After condensation the matrices become

$$\mathbf{U}_i = \begin{bmatrix} \mathbf{U}_B^{3\times 3} \otimes \mathbf{U}_A^{3\times 3} & \mathbf{0} \\ 0\ 0\ 0\ 0\ \sigma_A^{1/2}\sigma_B^{1/2}s_As_B\omega\ \ \sigma_B^{1/2}s_As_B\omega\ \ 0\ \ \sigma_A^{1/2}s_As_B\omega\ \ 0 & s_As_B\omega \end{bmatrix}_{i,\, i>x} \tag{2}$$

$$\mathbf{U}_x = \begin{bmatrix} \mathbf{U}_B^{3\times 3} \otimes \mathbf{U}_A^{3\times 3} & \begin{matrix} \sigma_A^{1/2}\sigma_B^{1/2}s_As_B\omega \\ 0 \\ \sigma_B^{1/2}s_As_B\omega \\ 0 \\ 0 \\ 0 \\ \sigma_A^{1/2}s_As_B\omega \\ 0 \\ 0 \end{bmatrix} \\ 0\ 0\ 0\ 0\ \sigma_A^{1/2}\sigma_B^{1/2}s_As_B\omega\ \ \sigma_B^{1/2}s_As_B\omega\ \ 0\ \ \sigma_A^{1/2}s_As_B\omega\ \ 0 & s_As_A\omega \end{bmatrix}_x \tag{3}$$

$$\mathbf{U}_i = \begin{bmatrix} \mathbf{U}_B^{3\times 3} \otimes \mathbf{U}_A^{3\times 3} & \begin{matrix} \sigma_A^{1/2}\sigma_B^{1/2}s_As_B\omega \\ 0 \\ \sigma_B^{1/2}s_As_B\omega \\ 0 \\ 0 \\ 0 \\ \sigma_A^{1/2}s_As_B\omega \\ 0 \\ 0 \end{bmatrix} \\ 0 & s_As_B\omega \end{bmatrix}_{i,\, i<x} \tag{4}$$

Here $\otimes$ denotes the direct product, $\mathbf{0}$ denotes a row or column composed of nine zeros, and ω is a factor that arises from orienting the cross-link so that helix propagation will result in helix alignment. Indexing of rows and columns for the matrix in eq 2 is $[c(c \text{ or } h)]_A[c(c \text{ or } h)]_B$, $(hc)_A[c(c \text{ or } h)]_B$, $(hh)_A[c(c \text{ or } h)]_B$, $[c(c \text{ or } h)]_A(hc)_B$, $[(h \text{ or } h^*)c]_A[(h \text{ or } h^*)c]_B$, $[(h \text{ or } h^*)h]_A[(h \text{ or } h^*)c]_B$, $[c(c \text{ or } h)]_A(hh)_B$, $[(h \text{ or } h^*)c]_A[(h \text{ or } h^*)h]_B$, $(hh)_A(hh)_B$, $(h^*h^*)_A(h^*h^*)_B$, while for the matrix in eq 4 the indexing is $[c(c \text{ or } h \text{ or } h^*)]_A[c(c \text{ or } h \text{ or } h^*)]_B$, $(hc)_A[c(c \text{ or } h)]_B$, $[h(h \text{ or } h^*)]_A[c(c \text{ or } h \text{ or } h^*)]_B$, $[c(c \text{ or } h)]_A(hc)_B$, $(hc)_A(hc)_B$, $(hh)_A(hc)_B$, $[c(c \text{ or } h \text{ or } h^*)]_A[h(h \text{ or } h^*)]_B$, $(hc)_A(hh)_B$, $(hh)_A(hh)_B$, $(h^*h^*)_A(h^*h^*)_B$. Rows in $\mathbf{U}_x$ are indexed as in eq 4, but the columns are indexed in the manner of eq 2.

Consequences of configurations of the types depicted in Figure 1C,D are incorporated in ω. A small value of ω would arise if there were many configurations of the type depicted in Figure 1C or if alignment of the helices was accompanied by the imposition of a stress at the cross-link site (Figure 1D). Physically, ω takes account of both modifications in the initiation parameter of the cross-linked residue relative to the non-cross-linked case as well as the enhanced (or reduced) statistical weight of a pair of helical residues at the cross-linked site in the dimer relative to the isolated monomer. Let $P_{hd}(x)$ be the statistical weight of a helix–helix pair at the cross-linked site x and $P_{hm}(x)$ the statistical weight of a helical residue x in the isolated monomer. Then $\omega = P_{hd}(x)[P_{hm,A}(x) \cdot P_{hm,B}(x)]^{-1}$. Observe that the quantitative (or even qualitative) effect of cross-linking on the values of the σ and s of cysteinyl residues is unknown. For this simple version of the theory the temperature dependence of ω should account for the "pretransition" seen in the thermal denaturation behavior of cross-linked tropomyosin. We shall address this point in detail in future work.

The configuration partition function, Z, is obtained as

$$Z = \mathbf{J}^*\mathbf{U}_1\mathbf{U}_2 \ldots \mathbf{U}_n\mathbf{J} \tag{5}$$

where $\mathbf{J}^*$ = row (1, 0, 0, 0, 0, 0, 0, 0, 0, 0) and $\mathbf{J}$ = col (1, 1, 0, 1, 1, 0, 0, 0, 0, 0). The probability that residue i in chain A is helical, P_{h,A_i}, is obtained as

$$P_{h,A_i} = Z^{-1}\mathbf{J}^*\mathbf{U}_1\mathbf{U}_2 \ldots \mathbf{U}_{i-1}\mathbf{U}'_i\mathbf{U}_{i+1} \ldots \mathbf{U}_n\mathbf{J} \tag{6}$$

where $\mathbf{U}'_i$ differs from $\mathbf{U}_i$ only in that all elements not containing s_A are made null. The helical content of chain A, $P_{h,A}$, is

$$P_{h,A} = n^{-1}\sum_{i=1}^{n} P_{h,A_i} \tag{7}$$

The helical content of the dimer, which we denote simply by p_h, is identical with $p_{h,A}$ if chain A and chain B have the same amino acid sequence.

Calculations were performed for various combinations of w and ω using the amino acid sequence of α-tropomyosin.[11,16] Each chain contains 284 amino acid residues, and the chains are assumed to be cross-linked at Cys-190. The σ and s values, collected in Table I, are those for water as the solvent and a temperature of 30 °C. They are taken from the experimental work of Scheraga and co-workers[17-33] or estimated by analogy with amino acid residues for which σ and s are known. After completion of the calculations reported here, experimental σ and s values were reported for glutamine.[34] Use of the experimental values in place of our estimates produces negligible effects on the calculations.

Table I
Statistical Weights Used for Amino Acid Residues (30 °C)

residue	$\sigma \times 10^4$	s	ref[a]
Ala	8	1.058	18
Asp	50	0.63	27
Glu, Gln	6	0.97	23
Phe, His	18	1.069	21
Gly	0.1	0.615	17
Ile	55	1.11	32
Lys	1	0.947	26
Leu	33	1.14	20
Met	54	1.15	29
Asn	0.1	0.806	28
Arg	0.01	1.017	26
Ser, Cys	0.8	0.793	19
Thr	0.1	0.836	30
Val	1	0.97	21,33
Trp	70	1.06	31
Tyr	66	0.96	24

[a] Reference for first amino acid residue listed.

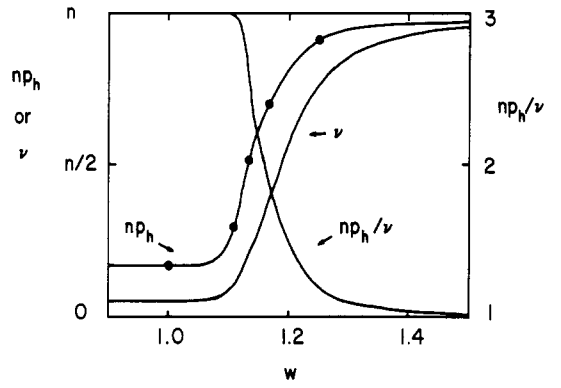

Figure 2. Average number of helical residues (np_h), average number of residues in a helical segment (ν), and average number of helical segments per chain (np_h/ν) for a cross-linked tropomyosin when $\omega = 1$.

Results and Discussion

Behavior When $\omega = 0$. If $\omega = 0$, the last row and last column in $\mathbf{U}_x$ are null. Since all terms in the last row and last column of each $\mathbf{U}_i$ are thereby rejected, the value assigned to w becomes irrelevant; i.e., the helices cannot interact. The configuration partition function for the cross-linked dimer depends only on $\mathbf{U}_A^{3\times3} \otimes \mathbf{U}_B^{3\times3}$; i.e., the configuration partition function reduces to the product of configuration partition functions for the isolated chains. This result arises because, if $\omega = 0$, the cross-link cannot adopt configurations that permit alignment and interaction of helices propagating away from the cross-link site. The completely helical dimer is forced into a configuration of the type depicted in Figure 1C. A calculation with $\omega = 0$ yields $p_h = 0.17$, and the average number of residues in a helical segment, ν, is 16.[8] The average number of helical segments in a chain, np_h/ν, is 3.

Behavior When $\omega = 1$. Figure 2 depicts the behavior of p_h, ν, and np_h/ν when ω is unity. If w is unity or smaller, the results are essentially those seen when $\omega = 0$. However, as w rises above 1.1, there is a dramatic increase in helical content. The helicity reaches 90% when w is 1.245. Associated with the increase in helicity, but lagging slightly behind, is an increase in the average number of residues in a helical segment. This number becomes equal to 90% of the residues in a tropomyosin chain when w is 1.35. The average number of helical segments in a polypeptide chain falls sharply from 3 to 1.5 as w rises from 1.1 to 1.2.

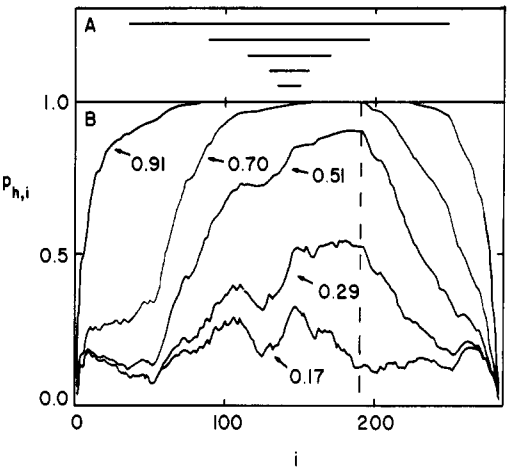

Figure 3. Average number of residues in a helical segment (A) and helix probability profile (B) for a cross-linked tropomyosin dimer when $\omega = 1$ and the helicity is 0.17, 0.29, 0.51, 0.70, or 0.91. Solid circles on the np_h line in Figure 2 denote these helicities.

Further increases in w are accompanied by a more gradual decline in np_h/ν. If w is as large as 1.5, nearly all chains contain one helical segment.

Five helix probability profiles are depicted in Figure 3B. The corresponding p_h are denoted by the five filled circles in Figure 2. A vertical line is drawn in Figure 3B at $i = 190$, which is the cross-link site. Figure 3A presents lines whose lengths are determined by ν. These lines are arbitrarily centered in the middle of the figure. Comparison of the helix probability profiles for the cases where p_h is 0.17 and 0.29 shows that the initial increase in helicity is confined to the vicinity of the cross-link site. The single residue whose helical content is enhanced the most is that residue that participates in cross-link formation. This observation is a necessary consequence of the conditions that must be met if the h* state is to be accessible to residue i. These conditions include the requirements that all residues from i through x be in the h* state. If the influence of the h* states is great enough (if w is large enough), the maximum in the helix probability profile must therefore shift to the cross-link site. This shift has occurred when $p_h = 0.51$ (Figure 3B). The helix probability profile at $p_h = 0.17$ contains much local detail, but this detail is obscured in the profile at $p_h = 0.51$. The requirement that residue i can be in the h* state only if residues i through x are all in this state demands that local detail must be lost as the h* state becomes dominant. The major differences in the helix probability profiles depicted in Figure 3A and those calculated earlier[33] lie in the location of the maximum and in the retention of local detail as p_h increases. These differences arise from the treatment of configurations of the type depicted in Figure 1E,F. The former is allowed in the earlier calculation, while the latter is allowed in the present treatment.

Helix formation by the ends of the tropomyosin chain lags appreciably behind that of the middle of the chain. The profile at $p_h = 0.51$ in Figure 3 shows that there has been almost no effect on the first 50 residues under conditions where $p_{h,x}$ is as large as 0.9. The last 20 residues also resist the imposition of a helical conformation. An alternative means of demonstrating these end effects is through specification of the w required to produce $p_{h,i} = {}^1/_2$. The necessary w are depicted in Figure 4. Much of the interior of the tropomyosin chain passes through the condition $p_{h,i} = {}^1/_2$ as w changes from 1.105 to 1.120. This portion nearly becomes helical as one unit. A smaller, but

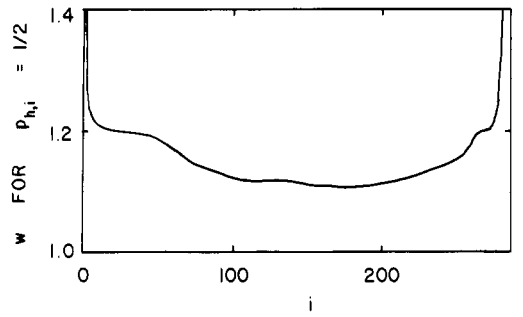

Figure 4. Values of w at which $p_{h,i}$ becomes $^1/_2$ for a cross-linked tropomyosin dimer with $\omega = 1$.

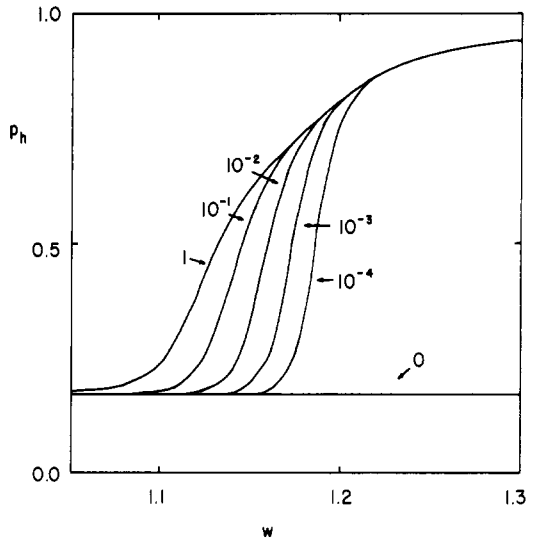

Figure 5. Helical content as a function of w for a cross-linked tropomyosin dimer when ω is 0, 10^{-4}, 10^{-3}, 10^{-2}, 10^{-1}, and 1, as indicated.

still significant, block near the amino terminus passes through the $p_{h,i} = {}^1/_2$ condition when w is 1.20. Appreciable helicity in this block, as well as in a smaller block at the carboxyl terminus, is developed only after the interior of the chain is completely helical, as is evident from the profile at $p_h = 0.70$ in Figure 3.

Variation of ω. The helical content is independent of w when $\omega = 0$ and strongly dependent on w when $\omega = 1$. Attention is now directed to circumstances where ω has an intermediate value. In these computations we are examining the consequences of configurations such as those depicted in Figure 1C,D. A small value for ω could arise if alignment of the helices requires a reduction in the configurational entropy of the cross-link or if cross-linking the helices produces strain.

Figure 5 depicts p_h as a function of w for six values of ω ranging from one to zero. The curve with $\omega = 1$ is taken from Figure 2. Three changes occur as ω decreases from 1 to 10^{-4}: First, the midpoint of the transition moves to higher w. Second, the transition becomes more cooperative; the slope becomes larger when $p_h = {}^1/_2$. Finally, while there is a large effect on the initial part of the transition, no effect whatsoever is seen in the final portion. That part of the transition for which $p_h > 0.7$ is unaffected when ω decreases from 1 to 0.1. The helix probability profiles depicted in Figure 3 show that it is the middle portion of tropomyosin that is affected as p_h rises from 0.17 to 0.7. Consequently, it is this portion whose helix formation has been rendered more difficult when ω falls from 1 to 0.1.

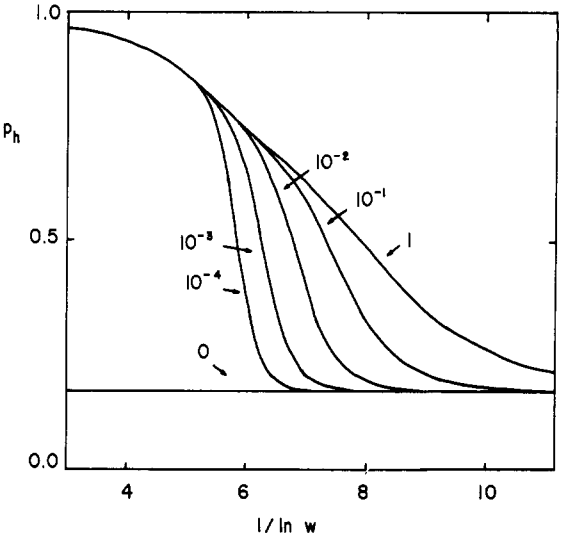

Figure 6. Helical content as a function of $1/(\ln w)$ for a cross-linked tropomyosin dimer when ω is 0, 10^{-4}, 10^{-3}, 10^{-2}, 10^{-1}, and 1, as indicated.

Figure 4 shows that the middle portion of the chain becomes helical nearly as one unit. Consequently, steric and/or entropic difficulties at the cross-link site will simply make helix formation by this block more difficult and more highly cooperative.

By way of illustration, if w is given by $\exp(-\Delta G/RT)$, with ΔH and ΔS independent of temperature, the influence of ω on the thermal profile is obtained from examination of p_h as a function of $1/(\ln w)$. In this approximation we ignore the temperature dependence of σ and s for the constituent amino acid residues. Data from Figure 5 are replotted in the prescribed manner in Figure 6. Curves depicted in Figure 6 clearly demonstrate that events at the cross-link site can have a profound influence on the high-temperature portion of the course of thermal denaturation of the cross-linked tropomyosin dimer. On the other hand, the low-temperature regime, where the parallel helical configuration of the dimer dominates, is essentially independent of ω.

Conclusion

The formulation of the configuration partition function for a cross-linked, in-register dimer has been refined so that it provides a more detailed treatment of the cross-link site and of the conditions necessary for helix–helix interaction by residues remote from the cross-link. When applied to tropomyosin, these refinements shift the location of the maximum in the helix probability profile to the residue at the cross-link site, suppress the local detail in the helix probability profile, and render more difficult the onset of helix formation. The proposed modifications should be most important for the high-temperature portion of the thermal denaturation of cross-linked tropomyosin.

Acknowledgment. This research was supported in part by Grant No. PCM-78-22916 from the National Science Foundation. Acknowledgment is also made to the donors of the Petroleum Research Fund, administered by the American Chemical Society, for partial support of this research.

References and Notes

(1) Cohen, C.; Szent-Gyorgyi, A. G. *J. Am. Chem. Soc.* **1957**, *79*, 248.
(2) Holtzer, A.; Clark, R.; Lowey, S. *Biochemistry* **1965**, *4*, 2401–2411.
(3) Woods, E. *Aust. J. Biol. Sci.* **1976**, *29*, 405–418.

(4) Lehrer, S. *J. Mol. Biol.* **1978**, *118*, 209–226.
(5) Edwards, F.; Sykes, B. *Biochemistry* **1980**, *19*, 2577–2583.
(6) Crimmins, D.; Isom, L.; Holtzer, A. *Comp. Biochem. Physiol. B* **1981**, *69B*, 35–46.
(7) Wu, C.-S.; Ikeda, K.; Yang, J.-T. *Biochemistry* **1981**, *20*, 566–570.
(8) Mattice, W. L.; Srinivasan, G.; Santiago, G. *Macromolecules* **1980**, *13*, 1254–1260.
(9) Hodges, R.; Sodek, J.; Smillie, L.; Jurasek, L. *Cold Spring Harbor Symp. Quant. Biol.* **1972**, *37*, 299–310.
(10) McLachlan, A.; Stewart, M. *J. Mol. Biol.* **1975**, *98*, 293–304.
(11) Stone, D.; Smillie, L. *J. Biol. Chem.* **1978**, *253*, 1137–1148.
(12) Mak, A.; Lewis, W.; Smillie, L. *FEBS Lett.* **1979**, *105*, 232–234.
(13) Skolnick, J.; Holtzer, A. *Macromolecules* **1982**, *15*, 303–314.
(14) Zimm, B.; Bragg, J. *J. Chem. Phys.* **1959**, *31*, 526–535.
(15) Skolnick, J., work in progress.
(16) Sodek, J.; Hodges, R. S.; Smillie, L. B. *J. Biol. Chem.* **1978**, *253*, 1129–1136.
(17) Ananthanarayanan, V. S.; Andreatta, R. H.; Poland, D.; Scheraga, H. A. *Macromolecules* **1971**, *4*, 417–424.
(18) Platzer, K. E. B.; Ananthanarayanan, V. S.; Andreatta, R. H.; Scheraga, H. A. *Macromolecules* **1972**, *5*, 177–187.
(19) Hughes, L. J.; Andreatta, R. H.; Scheraga, H. A. *Macromolecules* **1972**, *5*, 187–197.
(20) Alter, J. E.; Taylor, G. T.; Scheraga, H. A. *Macromolecules* **1972**, *5*, 739–745. van Wart, H. E.; Taylor, G. T.; Scheraga, H. A. *Ibid.* **1973**, *6*, 266–273.
(21) Alter, J. E.; Andreatta, R. H.; Taylor, G. T.; Scheraga, H. A. *Macromolecules* **1973**, *6*, 564–570.
(22) Maxfield, F. R.; Alter, J. E.; Taylor, G. T.; Scheraga, H. A. *Macromolecules* **1975**, *8*, 479–491.
(23) Scheule, R. F.; Cardinaux, F.; Taylor, G. T.; Scheraga, H. A. *Macromolecules* **1976**, *9*, 23–33.
(24) Dygert, M. K.; Taylor, G. T.; Cardinaux, F.; Scheraga, H. A. *Macromolecules* **1976**, *9*, 795–801.
(25) Kenishi, Y.; van Nispen, J. W.; Davenport, G.; Scheraga, H. A. *Macromolecules* **1977**, *10*, 1264–1271.
(26) Kobayashi, Y.; Cardinaux, F.; Zweifel, B. O.; Scheraga, H. A. *Macromolecules* **1977**, *10*, 1271–1283.
(27) Matheson, R. R., Jr.; Nemenhoff, R. A.; Cardinaux, F.; Scheraga, H. A. *Biopolymers* **1977**, *16*, 1567–1585.
(28) Hill, D. J.; Cardinaux, F.; Scheraga, H. A. *Biopolymers* **1977**, *16*, 2447–2467.
(29) Hecht, M. H.; Zweifel, B. O.; Scheraga, H. A. *Macromolecules* **1978**, *11*, 545–551.
(30) Nagy, J. A.; Powers, S. P.; Zweifel, B. O.; Scheraga, H. A. *Macromolecules* **1980**, *13*, 1428–1440.
(31) Fredrickson, R. A.; Chang, M. C.; Powers, S. P.; Scheraga, H. A. *Macromolecules* **1981**, *14*, 625–632.
(32) Chang, M. C.; Fredrickson, R. A.; Powers, S. P.; Scheraga, H. A. *Macromolecules* **1981**, *14*, 633–634.
(33) Skolnick, J.; Holtzer, A. *Macromolecules* **1982**, *15*, 812–821.
(34) Denton, J. B.; Powers, S. P.; Zweifel, B. O.; Scheraga, H. A. *Biopolymers* **1982**, *21*, 51.

Size and Solution Properties of Globular *tert*-Butyloxycarbonyl-poly(α,ϵ-L-lysine)

Shaul M. Aharoni,* Charles R. Crosby III, and Eugene K. Walsh

Corporate Research and Development, Allied Corporation, Morristown, New Jersey 07960.
Received December 23, 1981

ABSTRACT: Globular poly(α,ϵ-L-lysine) macromolecules protected on their surface by *tert*-butyloxycarbonyl residues were studied in dilute solution by means of viscosity determinations, photon correlation spectroscopy (PCS), and size exclusion chromatography (SEC). The three techniques yielded the following results: the homologues double their molecular weight with each incremented step, they are monodisperse, and the globular macromolecules are dense and behave as nondraining spheres. The sizes determined by viscosity and PCS are in agreement. In SEC they correlate well with the size of nondraining globular biopolymers. Globular poly(α,ϵ-L-lysine) macromolecules are thus suitable for use as molecular size "markers" in dilute solution studies of other polymers.

Introduction

Dense globular macromolecules of well-defined molecular weights, all with molecular weight distributions of $M_w/M_n = 1.0$, are usually biological in nature and obtained by extraction from living organisms. These biopolymers are usually soluble only in aqueous media. Furthermore, nature does not furnish us with globular macromolecules whose molecular weights and sizes change in uniform increments, making them suitable for studies of solution properties of dense globular macromolecules.

Denkewalter et al.[1] recently synthesized in our laboratories a series of *tert*-butyloxycarbonyl-blocked poly(α,ϵ-L-lysine) macromolecules. Models indicated them to be globular and dense. The molecular weight of each member of the series is twice that of the previous member. For each homologue the molecular weight distribution is extremely narrow, with $M_w/M_n \simeq 1.0$.

A detailed description of the synthetic procedure is presented in ref 1. The highlights of the procedure are summarized below. The nucleus of each globular macromolecule was *N*,*N*′-bis(*tert*-butyloxycarbonyl)-L-lysine benzhydrylamide. In reactions building on this nucleus, the nitrophenyl ester derivative of *N*,*N*′-bis(*tert*-butyloxycarbonyl)-L-lysine was found to be the most convenient reactive monomer. At each step, the Boc-protected product was deblocked in trifluoroacetic acid in dichloromethane, followed by the removal of excess acid and solvent under nitrogen. The resulting product was dissolved in dimethylformamide (DMF) and neutralized with triethylamine. A twofold molar excess (based on the calculated number of amino groups present) of Boc-L-NPE was added. The reaction mixture was then kept slightly basic by gradual addition of triethylamine. The reaction was allowed to proceed for 18 h in the case of the low molecular weight homologues and up to 3 days for the high molecular weight members of the series. The Boc-protected products were precipitated with ether, which allowed for the removal of excess reagents and byproducts. The Boc-protected products were then washed with acetonitrile and readied for the next synthetic step. For brevity, each member of the *tert*-butyloxycarbonyl-protected poly(α,ϵ-L-lysine) series was denoted by a symbol Boc-X. Thus the nucleus of each globular macromolecule was denoted by Boc-A, the second-stage product by Boc-B, the third-stage product by Boc-C, etc.

Because the Boc-X series was synthesized in a stepwise fashion with Boc-protected monomers, each member was expected to have a monodisperse molecular weight. Also,

0024-9297/82/2215-1093$01.25/0